Probe Molecule Kinetic Studies of Adsorption on MCM-41

Ángel Berenguer-Murcia,[†,‡] Ashleigh J. Fletcher,[†] Javier García-Martínez,[‡] Diego Cazorla-Amorós,[‡] Ángel Linares-Solano,[‡] and K. Mark Thomas*[,†]

Northern Carbon Research Laboratories, Department of Chemistry, Bedson Building, University of Newcastle-upon-Tyne, Newcastle-upon-Tyne NE1 7RU, U.K., and Departamento de Química Inorgánica, Universidad de Alicante, Apdo. 99, E-03080 Alicante, Spain

Received: August 15, 2002; In Final Form: October 29, 2002

Gases and vapors of varying dimensions were used as probes to investigate the adsorption processes on MCM-41 and precipitated silica, prepared by the same method as for MCM-41, but without the template. The adsorption kinetics of nitrogen, carbon dioxide, *n*-nonane, and α-pinene were studied for different amounts of preadsorbed gas/vapor as a function of relative pressure. The adsorption kinetics follow a linear driving force model for changes in surface coverage up to the adsorption isotherm plateaus. The variation of rate constant with relative pressure for MCM-41 and precipitated silica showed marked differences associated with adsorption in mesoporous structure, which are attributed to alignment of molecules in the mesopores leading to a pore blocking effect. The results are discussed in terms of differences in the adsorption mechanisms of gas/vapor diffusion in porous materials.

1. Introduction

MCM-41 is a mesoporous material, prepared by templating techniques, which belongs to the M41S family of materials.[1−5] It has a very narrow mesopore size distribution and a regular hexagonal array of unidimensional parallel channels. These materials are often referred to as ordered mesoporous materials (OMMs).[6] The pore sizes can be tailored in the range 1.4−10 nm, depending on the template and synthetic method used,[7,8] which makes the materials attractive for a variety of applications, including their use as adsorbents in the separation of large molecules and for environmental pollution abatement, and as catalysts or catalyst supports.[9−20]

Many different techniques have been employed to characterize the porous structure of MCM-41, including gas and vapor adsorption,[21−28] X-ray diffraction,[24,8−29] and spectroscopic methods.[30] Some authors have concluded that MCM-41 is an *exclusively* mesoporous material.[21,24,28,31] Adsorption studies have demonstrated novel effects, such as absence of hysteresis even when condensation-like transitions are observed.[32] However, whereas there have been a number of investigations of adsorption kinetics for gases/vapors on carbon molecular sieves,[33−41] active carbons,[42−46] and porous metal organic framework materials,[47] as far as we are aware, there have not been reports of similar investigations of adsorption dynamics for MCM-41 materials, which have a well-defined mesoporous structure.

The objective of this investigation was to compare the adsorption kinetics of a range of adsorptives with varying size and shape for mesoporous MCM-41 and precipitated silica (M001), prepared under identical conditions but without the templating agent, to establish the relation between sorption kinetics and the mesoporous structure. Comparisons of adsorptive size and pore dimensions were made to aid interpretation of the results.

2. Experimental

2.1. Adsorbent Synthesis. *MCM-41.* The synthesis was based on the method published previously.[48] Cetyltrimethylammonium bromide (4.8 g) was dissolved in 440 mL of distilled water. The mixture was stirred and heated gently until complete dissolution. NH_4OH (16 mL) was added, and the resulting mixture was stirred at 380 rpm for 5 min. Tetraethoxysilane (20 mL) was added and the solution stirred at 380 rpm for 1 h. The mixture was filtered and dried overnight at 323 K.

Precipitated Silica M001. The synthesis of the precipitated silica was carried out using a method similar to MCM-41, but without adding the template (cetyltrimethylammonium bromide). Ethanol was added to precipitate the silica.

Calcination. The samples were heated at 5 K min^{-1} in N_2 (flow rate: 100 mL min^{-1}) to 823 K with a hold time at the heat treatment temperature (HTT) of 1 h. The nitrogen flow was switched to oxygen and the sample was calcined for 5 h at 823 K before cooling to ambient temperature.

2.2. X-ray Diffraction Studies. X-ray diffraction measurements for the samples were performed using a Seifert 2002 powder diffractometer using Cu Kα radiation (1.54 Å).

2.3. Scanning Electron Microscopy. Scanning electron micrographs (SEMs) were obtained using a JEOL electron microscope (Model 5300LV).

2.4. Adsorption Studies. *Adsorption Isotherms.* Nitrogen adsorption studies at 77 K were carried out using either a Quantachrome Autosorb-6 adsorption system or a Hiden Analytical Intelligent Gravimetric Analyzer. Carbon dioxide adsorption at 273 K and <1 bar was measured using a Coulter Omnisorp 610 and Hiden Analytical Intelligent Gravimetric Analyzer.

Adsorption at High Pressure. High-pressure carbon dioxide adsorption/desorption studies at 273 K were carried out using a Sartorius 4406 DMT high-pressure microbalance. The samples

* To whom all correspondence should be addressed: E-mail: mark.thomas@ncl.ac.uk.
† University of Newcastle-upon-Tyne.
‡ Universidad de Alicante.

10.1021/jp026764d CCC: $25.00
Published on Web 01/01/2003

~160 mg were degassed for 6 h at 523 K at a pressure of 1×10^{-6} Pa. The buoyancy corrections due to the sample holder and pan were obtained using a blank experiment carried out with the sample holder containing only the glass wool used to avoid the loss of sample due to pressure changes. Adsorption and desorption isotherms were measured up to ~25.5 bar pressure ($p/p^0 = 0.73$).

Adsorption Kinetic Studies. An Intelligent Gravimetric Analyzer (IGA) supplied by Hiden Analytical Ltd., U.K., was used in this study. This apparatus is an ultrahigh vacuum system, which allows isotherms and the corresponding kinetics of adsorption and desorption to be determined, for set pressure steps.[38−47,49] The balance and pressure control system were fully thermostated to ±0.2 K to eliminate changes in the external environment. The microbalance had a long-term stability of ±1 μg with a weighing resolution of 0.2 μg. The adsorbent sample (100 ± 1 mg) was outgassed until constant weight, at a pressure of $<10^{-6}$ Pa at 473 K. The sample temperature for vapor adsorption was controlled to ±0.1 K by a computer-controlled bath circulating a 1:1 mixture of ethylene glycol and water around the stainless steel sample chamber. The sample temperature was monitored throughout the experiment and the variation in sample temperature was minimal (<0.1 K). The first pressure increment involves a change from ultrahigh vacuum to gas/vapor, and this introduces conduction through the gas phase to the sample, which results in a slightly larger temperature variation until equilibrium is restored. The sample temperature for nitrogen adsorption was achieved using an extended quartz sample vessel and hangdown with liquid nitrogen in a Dewar flask. The liquid used to generate the adsorptive vapors was degassed fully by repeated evacuation and vapor equilibration cycles of the liquid supply side of the vapor reservoir. The vapor pressure was gradually increased, over a time-scale of ~30 s to prevent disruption of the microbalance, until the desired value was achieved. Pressure control was via the use of three transducers with ranges 0−0.2, 0−10, and 0−200 kPa, each with an accuracy of 0.02% of the specified range. The pressure was maintained at the set point by active computer control of the inlet/outlet valves throughout the duration of the experiment. The mass uptake was measured as a function of time and the approach to equilibrium of the mass relaxation curve monitored in real time using a computer algorithm. After equilibrium was established, the vapor pressure was increased to the next set pressure value and the subsequent uptake was measured until equilibrium was reestablished. The increase in weight due to adsorption for each pressure step was used to calculate the kinetic parameters for adsorption using an appropriate kinetic model. The use of small pressure increments minimizes effects due to heat of adsorption. A thermocouple located very close to the sample showed no temperature changes resulting from the pressure increments. The errors in the calculated rate constants were typically better than ±2%.

The saturated vapor pressures were calculated using the following equation[50,51]

$$\log_{10} p = A - \frac{B}{T + C} \quad (1)$$

where p is the saturated vapor pressure (Torr), T is the temperature in degrees Celsius and A, B, and C are constants defined by the adsorbate: nitrogen (77−373 K) $A = 6.49457$, $B = 255.68$, $C = 266.550$, carbon dioxide (77−303 K): $A = 7.810237$, $B = 995.7048$, $C = 293.4754$; *n*-nonane (312−452 K): $A = 6.93893$, $B = 1431.82$, $C = 202.01$; α-pinene (292−429 K): $A = 6.8525$, $B = 1446.4$, $C = 208.0$.

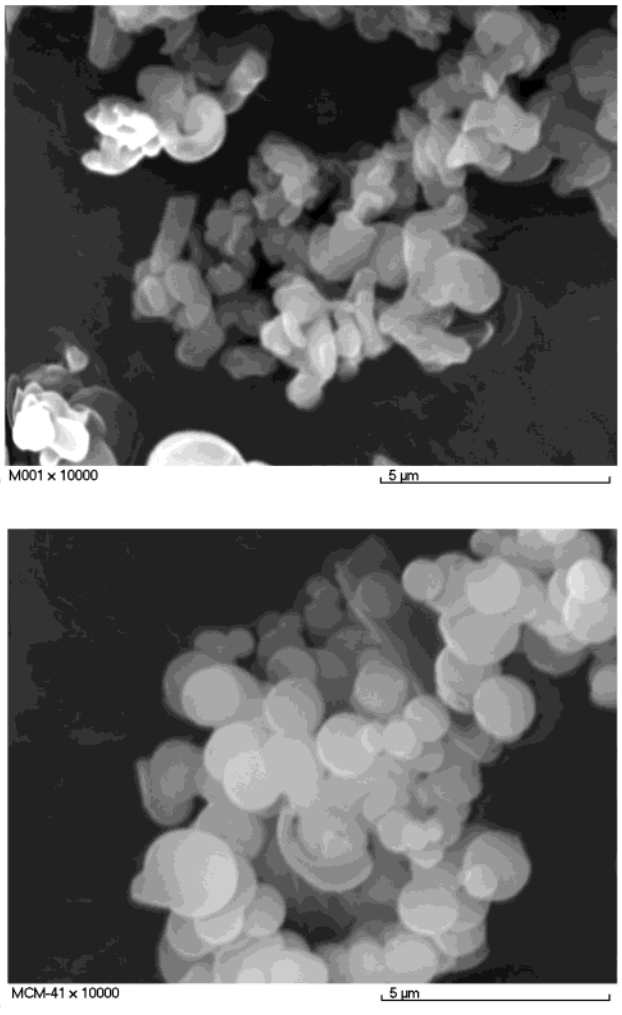

Figure 1. Scanning electron micrographs of (a) M001 and (b) MCM41.

3. Results

3.1. Particle Size and Morphology. Typical scanning electron micrographs of M001 and MCM-41 are shown in Figure 1a,b, respectively. It is apparent that particles of both M001 and MCM-41 occur as agglomerates with the particle size distributions being quite similar and typically in the size range ~0.5−1.5 μm. The particles of MCM-41 are approximately spherical in shape whereas those of M001 are more irregular. Scanning electron micrographs of M001 and MCM-41 at lower magnification, showing the range of size of the agglomerates, are given in the Supporting Information. It is apparent that M001 and MCM-41 have similar particle size and agglomerate size characteristics.

3.2. X-ray Diffraction. Figure 2 shows the diffractogram obtained for the MCM-41 sample used in this study. Three peaks were observed, a main peak at $2\theta \sim 2.5°$ corresponding to the 100 plane of MCM-41 (which gives a value of d_{100} of 3.37 nm) and two smaller peaks at $2\theta \sim 4.3°$ and 4.7° corresponding to the 110 and 200 planes of MCM-41. The presence of these smaller peaks confirms that long-range order was present in the sample. It is apparent that the sample was MCM-41 without any lamellar phase impurities. M001 does not have any X-ray diffraction peaks, which is consistent with it being amorphous.

3.3. Adsorption Isotherm Measurements. The adsorption isotherms for nitrogen (77 K), carbon dioxide (273 K), *n*-nonane (313 K), and α-pinene (313 K) on M001 are shown in Figure

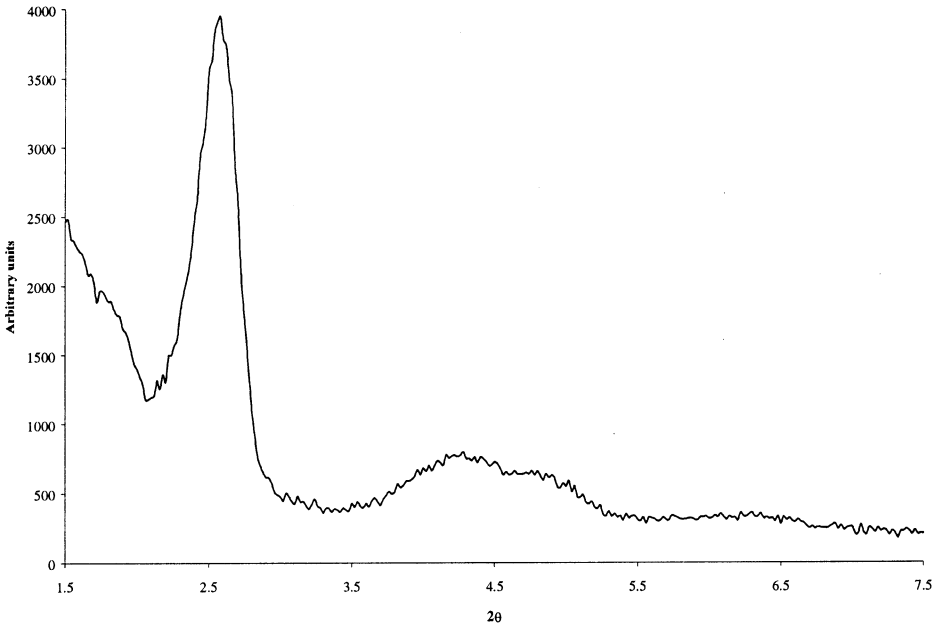

Figure 2. X-ray diffractogram of the MCM-41 used in this study

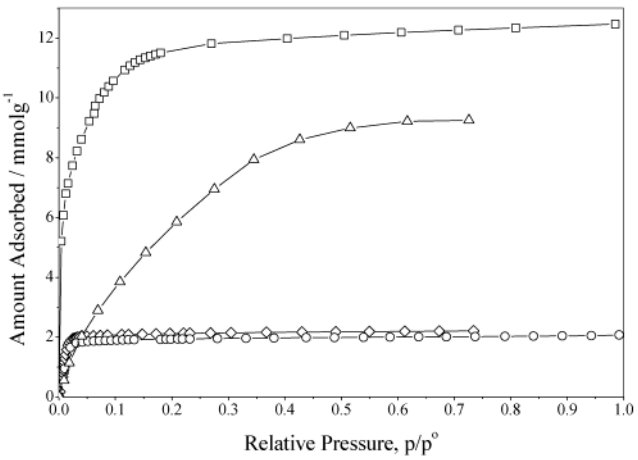

Figure 3. Adsorption isotherms for (a) nitrogen (□, 77 K), (b) carbon dioxide (△, 273 K), (c) *n*-nonane (○, 313 K), and (d) α-pinene (◇, 313 K) on precipitated silica M001.

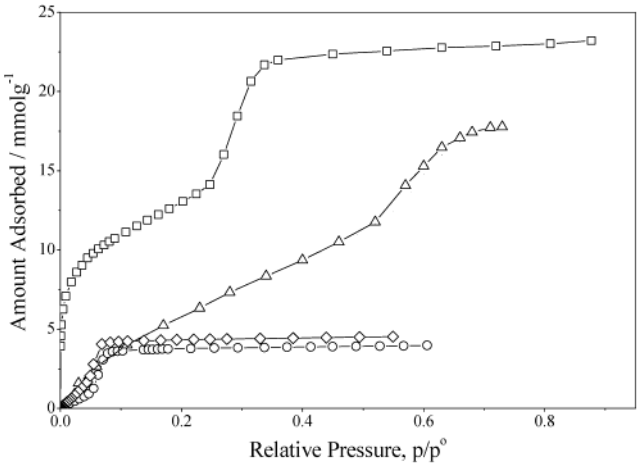

Figure 4. Adsorption isotherms for (a) nitrogen (□, 77 K), (b) carbon dioxide (△, 273 K), (c) *n*-nonane (○, 313 K), and (d) α-pinene (◇, 313 K) on MCM-41.

3. It is apparent that all four isotherms are type 1 in the IUPAC classification scheme. The total pore volumes obtained from extrapolation of the adsorption plateaus at high relative pressure gave the following values: nitrogen 0.432 $cm^3\ g^{-1}$ ($\rho_{nitrogen} = 0.8081\ g\ cm^{-3}$), carbon dioxide 0.398 $cm^3\ g^{-1}$ (obtained from uptake at p/p^0 0.726 with $\rho_{CO_2} = 1.023\ g\ cm^{-3}$), *n*-nonane 0.371 $cm^3\ g^{-1}$ ($\rho_{n-nonane} = 0.7176\ g\ cm^{-3}$), and α-pinene ~0.350 $cm^3\ g^{-1}$($\rho_{\alpha-pinene} = 0.8582\ g\ cm^{-3}$).

The adsorption isotherms for nitrogen, carbon dioxide, *n*-nonane, and α-pinene on MCM-41 are shown in Figure 4. The nitrogen adsorption isotherm is in excellent agreement with previous studies.[24] The isotherm is very steep at low relative pressure followed by a point of inflection at $p/p^0 \sim 0.1$ and another steep uptake followed by a plateau for $p/p^0 > 0.375$.

Comparison of the set of adsorption isotherms shows that they have a similar shape with a shoulder. The shoulder is less pronounced and at much lower relative pressure for *n*-nonane and α-pinene compared with nitrogen whereas the shoulder in the carbon dioxide isotherm is at higher relative pressure than in the nitrogen adsorption isotherm. The carbon dioxide adsorption/desorption isotherms do not show significant hysteresis.

The total pore volumes were obtained from linear extrapolation of the adsorption plateaus at high relative pressure. The nitrogen pore volume of virgin MCM-41 was 0.766 $cm^3\ g^{-1}$ whereas the nitrogen pore volumes determined after measurements of adsorption isotherms of *n*-nonane and α-pinene were 0.811 and 0.805 $cm^3\ g^{-1}$, respectively. This small increase in pore volume possibly indicates a minor structural change as a result of adsorption, but the changes are close to the experimental errors with the plateau being repeatable to ~±0.01 $cm^3\ g^{-1}$. The total pore volumes obtained for carbon dioxide, *n*-nonane, and α-pinene adsorption were 0.765, 0.732, and 0.717 $cm^3\ g^{-1}$, respectively. However, the high-pressure carbon dioxide isotherm limit was 25.5 bar and the pore volume was calculated from the amount adsorbed at this pressure because of the uncertainty in extrapolation of a limited amount of data relating to the plateau. It is evident that the total pore volumes for both M001 and MCM-41 were in the order: nitrogen > carbon dioxide > *n*-nonane ~ α-pinene and that there is a small deviation from Gurvitch's rule.

3.4. Adsorption Kinetics. The linear driving force (LDF) model is followed for substantial parts of the adsorption isotherms of a wide range of gases and vapors on carbon molecular sieves (CMS),[33,38−41] active carbons,[42−46] and metal

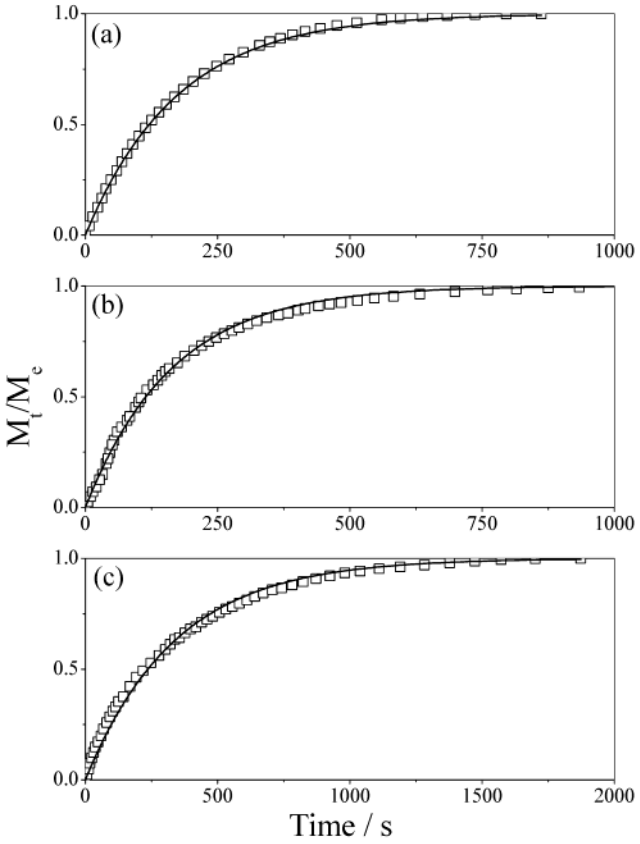

Figure 5. Adsorption kinetics profiles for (a) nitrogen (p/p^0 0.1292−0.1933, 77 K, every 7th point only, line is LDF model fit) (b) *n*-nonane (p/p^0 0.01716−0.02560, 313 K, every 22nd point only, line is LDF model fit), and (c) α-pinene (p/p^0 0.007858−0.08660, 313 K, every 10th point only, line is LDF model fit) on precipitated silica M001.

organic framework materials[47] and is described by the equation

$$\frac{M_t}{M_e} = 1 - e^{-kt} \qquad (2)$$

where M_t is the uptake at time t, M_e is the equilibrium uptake, and k is the rate constant. The rate constant can be obtained either from a plot of $\ln(1 - M_t/M_e)$ versus time, which is linear with a gradient equal to the rate constant, or by fitting the graph of M_t/M_e versus time curve to the equation.

Figure 5 shows graphs of M_t/M_e versus time for typical adsorption steps for nitrogen (77 K), *n*-nonane (313 K), and α-pinene (313 K) on the precipitated silica M001 together with the corresponding fits for the LDF model. It is evident that the adsorption kinetics for the three adsorptives obey the LDF model for >90% of the total uptake for a particular pressure step. Carbon dioxide adsorption on M001 at 273 K also follows the LDF model up to $p/p^0 \sim 0.03$ with rate constants typically $>1 \times 10^{-2}$ s^{-1}. Kinetic measurements could not be obtained from the high-pressure carbon dioxide adsorption studies because of the lack of control of the pressure setting process.

Figure 6 shows graphs of M_t/M_e versus time for typical adsorption steps for nitrogen, *n*-nonane and α-pinene on virgin MCM-41 and the corresponding fits for the LDF model. It is apparent that the adsorption kinetics also obey the LDF model.

The nitrogen adsorption will be considered separately because of the slightly higher pore volume observed compared with *n*-nonane and α-pinene. Figure 7 shows a comparison of the variation of adsorption rate constants with relative pressure for

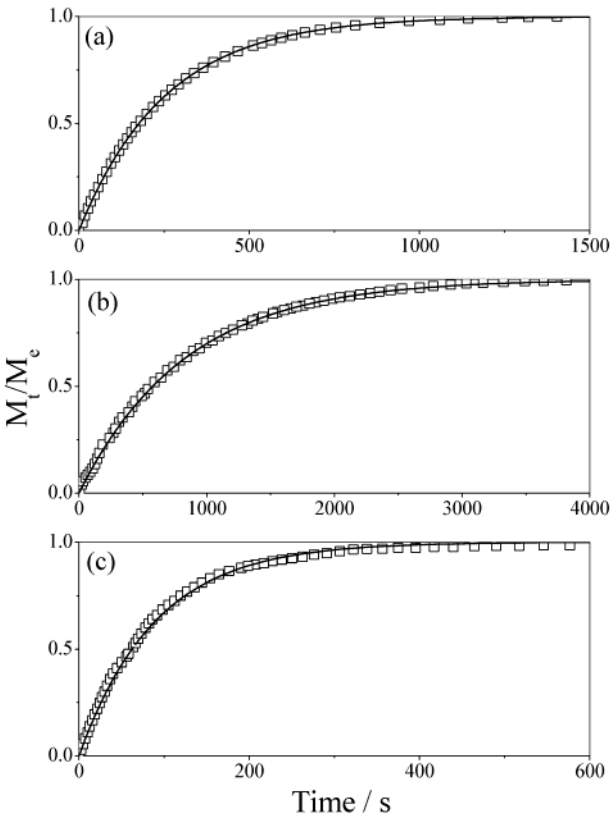

Figure 6. Adsorption kinetic profiles for nitrogen (p/p^0 0.2582−0.3226, 77 K, every 10th point only, line is LDF model fit), *n*-nonane (p/p^0 0.06105−0.07076, 313 K, every 24th point only, line is LDF model fit), and α-pinene (p/p^0 0.005349−0.007225, 313 K, every second point only, line is LDF model fit) on MCM-41.

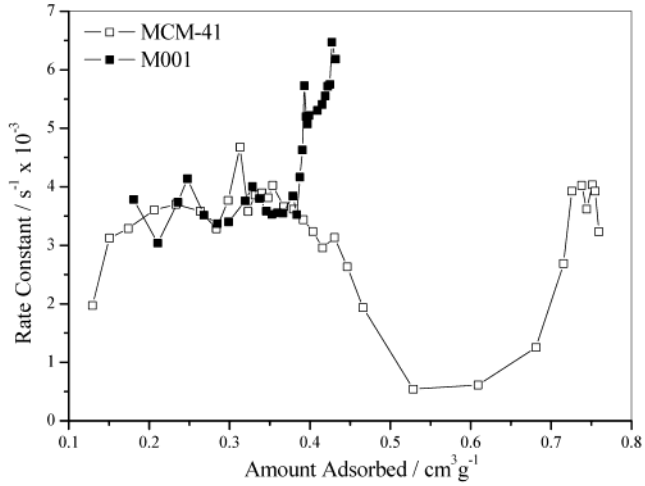

Figure 7. Variation of rate constant with relative pressure for nitrogen adsorption on M001 and MCM-41 at 77 K.

adsorption of nitrogen on M001 and virgin MCM-41 at 77 K. In this graph the final equilibrium relative pressures for the pressure increments were used whereas the kinetic measurements refer to the pressure increment. In the case of M001 the first pressure step ($p/p^0 = 0.004\,01$) represents ∼41.8% of the total uptake of nitrogen. If the graph is plotted on a rate constant versus amount adsorbed basis, the rate constants do not change up to ∼80% of the total pore volume but increase dramatically thereafter. The rate constants start at $\sim 3 \times 10^{-3}$ s^{-1} and increase to $\sim 6 \times 10^{-3}$ s^{-1} at high relative pressure. The corresponding trend in the variation of rate constant with relative pressure for MCM-41 is markedly different. Initially, the rate constants are

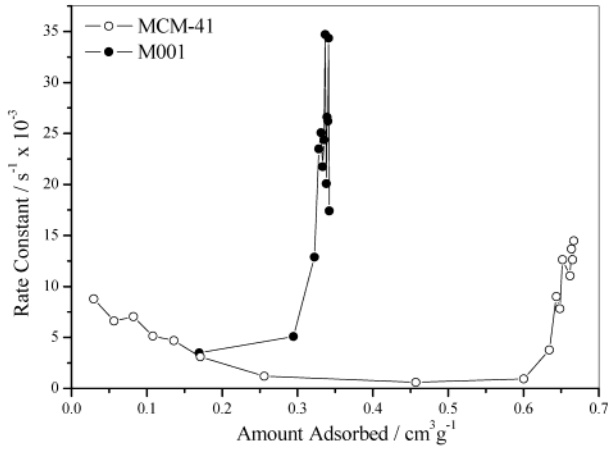

Figure 8. Variation of rate constant with relative pressure for *n*-nonane adsorption on M001 and MCM-41 at 313 K.

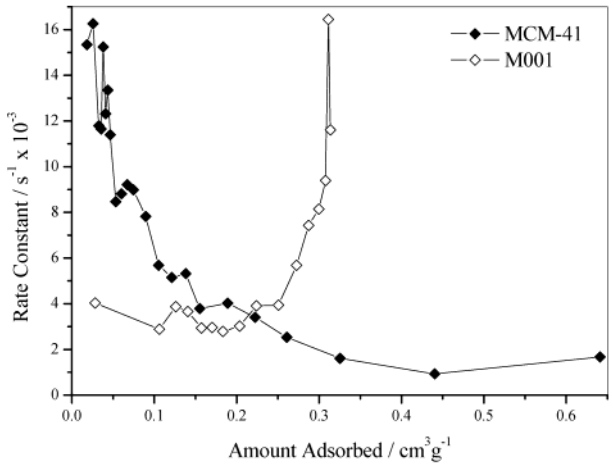

Figure 9. Variation of rate constant with relative pressure for α-pinene adsorption on M001 and MCM-41 at 313 K.

similar to those obtained for M001 varying in the range ~3 × 10^{-3} to ~4 × 10^{-3} s^{-1} for $p/p^0 \sim 0-0.15$ before decreasing to 5 × 10^{-4} s^{-1} at $p/p^0 \sim 0.28$. The rate constants increase rapidly thereafter, reaching a plateau with $k \sim 4 \times 10^{-3}$ s^{-1} for $p/p^0 >$ 0.375. Hence, initially the rate constants for MCM-41 are similar to those for M001 but a distinct slowing down occurs in the region of the point of inflection of the MCM-41 isotherm where the mesoporous structure is close to being filled.

The variation of rate constants with relative pressure for adsorption of *n*-nonane on M001 and MCM-41 are shown in Figure 8. The values obtained at 313 K for *n*-nonane adsorption on M001 range initially from 3 × 10^{-3} s^{-1} to 35 × 10^{-3} s^{-1} at $\sim p/p^0 = 0.12$ whereas the corresponding values for MCM-41 start initially at ~9 × $10^{-3}$$s^{-1}$ and decrease to 6 × 10^{-4} s^{-1}at $p/p^0 \sim 0.065$ before increasing to ~12 × 10^{-3} s^{-1} at $p/p^0 \sim$ 0.1. The minimum corresponds to the start of the second steep uptake in the isotherm and to ~63% of the total pore volume whereas the plateau in the rate constants coincides with the isotherm plateau.

The variation of rate constants with relative pressure for adsorption of α-pinene on M001 and MCM-41 are shown in Figure 9. Adsorption of α-pinene on M001 also shows similar trends of increasing rate constant with increasing relative pressure with the rate constant initially in the range 3 × 10^{-3} to 4 × 10^{-3} s^{-1} for the p/p^0 range 0−0.015 increasing to ~1.4 × 10^{-2} s^{-1} at $p/p^0 = 0.028$ corresponding to ~90% of the α-pinene total pore volume. In contrast, the rate constants

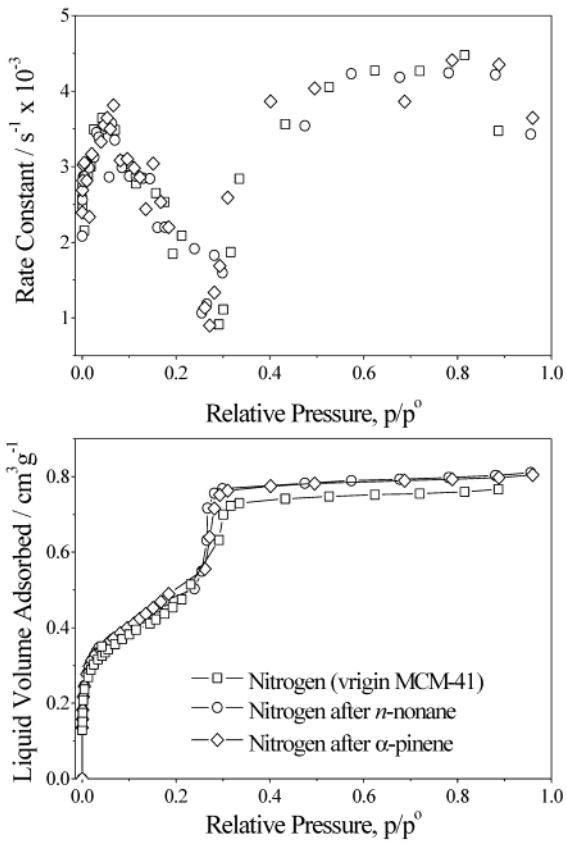

Figure 10. Comparison of nitrogen adsorption isotherms and kinetic rate constants for MCM-41 at 77 K: (a) virgin MCM-41 (□), (b) after *n*-nonane (○) preadsorption at 313 K, and (c) after α-pinene (◇) preadsorption at 313 K.

for α-pinene adsorption on MCM-41 were initially 1.6 × 10^{-2} s^{-1} and decreased to ~1 × 10^{-3} s^{-1} at $p/p^0 \sim 0.055$ (uptake = ~61.5% of the α-pinene total pore volume) before increasing to ~1.4 × 10^{-3} s^{-1} at $p/p^0 > 0.069$ (uptake 89.5% of the α-pinene total pore volume). There is a very large uptake for the pressure increment 0.1−0.125 kPa, which corresponds to ~28% of the total uptake. The minimum in the rate constant versus relative pressure graph occurs at the beginning of the steepest part of the isotherm similar to kinetics for *n*-nonane adsorption on MCM-41. Therefore, for both *n*-nonane and α-pinene adsorption, the rate constants are initially faster for MCM-41, but the different trends in rate constant with relative pressure for M001 and MCM-41 lead to rate constants for adsorption on M001 being greater than MCM-41 at higher relative pressure.

Small increases in total pore volumes for MCM-41 obtained from nitrogen adsorption at 77 K were observed after both *n*-nonane and α-pinene adsorption at 313 K. The nitrogen adsorption isotherms at 77 K for virgin MCM-41, and MCM-41 after *n*-nonane and α-pinene preadsorption, and the corresponding variation in rate constant with relative pressure are shown in Figure 10. It is apparent that both the isotherms and kinetic data are very similar, indicating only very minor differences due to structural relaxation.

4. Discussion

4.1. X-ray Diffraction Analysis. The pore radius (r_1) and theoretical pore volume (PV_{theo}) were calculated from the X-ray diffraction data for MCM-41 from geometric considerations using an hexangonal pore array, the Kelvin−Cohan equation,

TABLE 1: Molecular Sizes (pm) of the Adsorptives Used in This Study

	MIN-1	MIN-2	MIN-3
CO_2[a]	318.9	333.9	536.1
N_2[a]	299.1	305.4	404.6
n-C_9H_{18}[a]	401.4	452.4	1407.6
CH_3OH[b]	381.0	418.0	495.0
α-$C_{10}H_{16}$[c]	677.0	691.0	858.0

[a] Reference 53. [b] Reference 54, calculated by Dr. C. E. Webster and Dr. M. C. Zerner by ZINDO methods used in ref 53. [c] Calculated by Dr. Ted O"Brien.[55]

and the statistical thickness of the adsorbed wall was obtained using the t-method. The values obtained for r_1 and PV_{Theo} were 1.44 nm and 0.44 cm^3 g^{-1}, respectively. The ranges of values for r_1 and PV_{Theo} given in the literature were 1.42−2.06 nm and 0.31−0.59, respectively.[27−29,48,52] These structural characteristics are typical of those found in the literature for MCM-41.

4.2. Adsorption Isotherms. Adsorption on porous materials involves diffusion through a porous system, which may, in the two extreme situations, have either slit shaped or spherical characteristics. In the case of the former, only one adsorptive dimension is critical in determining the adsorption characteristics, whereas for the latter, two dimensions need to be considered. The molecular dimensions obtained from ZINDO calculations[53−55] for the suite of adsorptives used in this study are given in Table 1. Other estimates of molecular dimensions are also available for comparison.[56] It is apparent from the ZINDO calculations that the adsorptives used in this study have markedly different sizes with cross-sectional minimum dimensions in the range from ∼299−305 for nitrogen to 677−691 pm for α-pinene.

Previous workers have reported the synthesis of M41S materials with varying amounts of template and the corresponding nitrogen adsorption isotherms (77 K).[57] The initial uptake isotherm remained unchanged whereas the second uptake plateau was directly related to the amount of template used. The nitrogen adsorption isotherms (77 K) for various M41S series porous materials with different templates have also been reported.[27] This study showed that the point of inflection ($p/p^0 < 0.1$) was independent of the template whereas the plateau at $p/p^0 \sim 0.3$ varied with the template used. It is apparent that the second uptake is strongly related to the porosity resulting from the template used in the synthesis of the material.

The MCM-41 isotherms do not increase so sharply at low relative pressure for *n*-nonane and α-pinene compared with the M001 isotherm, and there are points of inflection corresponding to the start of filling of mesoporosity for all three adsorptives. The steeper M001 isotherm at low relative pressure indicates that the porosity accessed by *n*-nonane and α-pinene in MCM-41 is wider than M001.

The total pore volumes for M001 from *n*-nonane and α-pinene adsorption are ∼14 and 19% lower than the nitrogen pore volume for the M001 sample. Also, the pore volumes for MCM-41 from *n*-nonane and α-pinene adsorption are ∼10−11% lower than the nitrogen pore volume for the MCM-41 sample. Previous studies have also shown that the MCM-41 isotherm plateaus for a range of adsorptives were almost identical but also lower than the corresponding nitrogen isotherm plateau. It was proposed[27] that because methanol and nitrogen had similar sizes, this difference in the amount adsorbed was due to the much lower temperatures used for nitrogen adsorption.

The *n*-nonane and α-pinene pore volumes for MCM-41 were 10−11% lower than the nitrogen pore volumes measured after the adsorption of these vapors and also, ∼5% lower than the nitrogen pore volume for virgin MCM-41. Possible reasons for the lower *n*-nonane and α-pinene pore volumes observed for both M001 and MCM-41 are (a) exclusion of the larger adsorptives from part of the porous structure, (b) inaccurate or inappropriate density for some of the adsorbates, (c) surface structure effects, and (d) packing differences in the porosity. However, it is difficult to distinguish between these alternatives by comparison with other porous systems.

Carbon molecular sieve (CMS) materials are used for air separation based on differences in the adsorption kinetics but amounts adsorbed at equilibrium are similar.[41] Large molecules, such as benzene (327.7 × 662.8 × 773.7 pm), are excluded from part (∼60%) of the porous structure of these materials by the selective porosity in the CMS, which behaves as though it had spherical characteristics.[41] Carbon dioxide and nitrogen are smaller and have quite similar minimum dimensions (see Table 1) and are not excluded from the CMS when adsorbed at ambient temperature. However, adsorption of nitrogen at 77 K has kinetic limitations, which result in a very low uptake at 77 K. These very slow kinetics were not observed for M001 and MCM-41 (see discussion later). The similarity between the pore volumes for *n*-nonane and α-pinene, which have markedly different dimensions (see Table 1) indicate that there is no exclusion from the porous structure due to size effects over the 400−700 pm size range. It can be argued that the total pore volumes from carbon dioxide adsorption at 273 K are underestimates because of the pressure limit (25.5.bar) and that carbon dioxide and nitrogen, which have similar cross-sectional dimensions, also have similar total pore volumes. This explanation involving exclusion for part of the porous structure is difficult to justify unequivocally, bearing in mind the small differences, the extrapolation of the data, and the uncertainties in the density of the adsorbed phase and molecular packing effects.

The density of the adsorbed phase is not known with high accuracy and liquid densities are usually used to calculate the total pore volumes. However, there are some notable exceptions to this rule. The density of adsorbed water on active carbon is usually lower than the liquid density due to the inability of adsorbed water to form a full 3-dimensional structure in the microporosity.[42,42,58] The nitrogen-adsorbed phase may also be more solidlike, leading to the adsorbate density being higher than the expected liquid density.[59] However, the nitrogen pore volume and organic liquid pore volumes usually agree well for active carbon; for example, the nitrogen, *n*-nonane,[45]and α-pinene[60] pore volumes are 0.83, 0.89, and 0.87 cm^3 g^{-1}, respectively, for BAX950. Adsorption of other molecules on BAX950 gave values of 0.84 cm^3 g^{-1} for methanol, ethanol, propan-1-ol, and butan-1-ol, 0.85 cm^3 g^{-1} for *n*-octane,[45] 0.86 cm^3 g^{-1} for chlorobenzene, 0.87 cm^{3}g^{-1} for benzene, and 0.89 cm^3 g^{-1} for 1,3 dichlorobenzene and 2-chlorotoluene.[60] This detailed comparison for adsorption of 12 gases/vapors on active carbon showed that the use of the liquid densities for nitrogen (77 K) and organic vapor pore volumes (288−318 K) gave a pore volume range of 0.06 cm^3 g^{-1} (average 0.86 ± 0.02 cm^3 g^{-1}) with all the pore volumes for organic liquids being higher than for nitrogen, which had the lowest value. It is evident that in this case the difference in adsorption temperatures was not a major factor. In contrast, the *n*-nonane and α-pinene total pore volumes are 0.079−0.088 cm^3 g^{-1} or (∼10−11%) lower than the nitrogen pore volume measured after adsorption of the organic vapor. Therefore, an effect of temperature as the sole factor in controlling the adsorbate density is difficult to sustain.

M001 and MCM-41 have similar trends in pore volumes but quite different pore structures, and therefore, an effect specifically linked to porosity is unlikely. However, the structure of the pore wall material in M001 is very similar to that of MCM-41. It is also possible that the surface structure influences the density of the adsorbed phase in these materials. It is noteworthy that the amount of exclusion for M001 is approximately twice that for MCM-41 on a relative basis but approximately the same on an absolute basis. This suggests that the pore wall material in MCM-41 is a factor. Therefore, the explanation for the higher nitrogen pore volumes of the adsorptives studied on M001 and MCM-41 is equivocal.

4.3. Adsorption Kinetics. Rao et al. developed a model[61,62] for the interaction potential of diffusing species in porous carbon molecular sieves and concluded that two processes are involved in the adsorption dynamics: (a) diffusion along the pores and (b) diffusion through the barrier at the pore entrance. A LDF model is followed when the latter is the rate-determining step and a Fickian diffusion model when the former controls the kinetics. Adsorption of gases/vapors on carbon molecular sieves,[38−41] active carbons,[42−46] and metal organic framework materials[47] usually obey the LDF model for substantial parts of the isotherms. In the case of adsorption on carbon molecular sieves prepared by carbon deposition, this barrier results from constrictions in the porosity caused by the heterogeneous distribution of deposited carbon.[63] The kinetic selectivity of the CMS for gases/vapors, for example, oxygen and nitrogen, is controlled by the deposited carbon, which forms the selective porosity. The adsorption rate constants decrease by 4 orders of magnitude for adsorptives with dimensions increasing in the size range 300−400 pm before partial exclusion begins at ∼400 pm followed by exclusion of adsorptive molecules with dimensions greater than ∼550 pm from 60% of the porous structure.[41] The adsorption kinetics for the excluded molecules are faster than when the adsorptives pass through the selective porosity because the barriers are lower in the nonselective porosity.

The adsorption kinetics for all the adsorptives on both M001 and MCM-41 followed a linear driving force model over the complete pressure ranges studied. These observations are consistent with diffusion through a barrier being the rate-determining step. The rate constants are similar to those observed for diffusion of gases and vapors into carbon molecular sieves, active carbons and metal organic framework molecules.[38−47] These rate constant values compare well with rate constants increasing with increasing relative pressure and surface coverage from 6×10^{-4} to 97×10^{-4} s^{-1} at 313 K for adsorption of *n*-nonane on active carbon BAX950.[45] It is evident that the trends in rate constant with relative pressure and surface coverage are similar for M001 and active carbon BAX950 and the rate constants for adsorption of *n*-nonane adsorption on M001 are significantly faster than those for active carbon BAX950 at low surface coverage.[44,45]

Low Surface Coverage. The adsorptives studied cover a wide size range with the two minimum cross-sectional dimensions in the ranges ∼299−677 and ∼305−692 pm, respectively. The adsorption kinetics follow the LDF model at low surface coverage, which indicates the presence of a barrier to diffusion in the porous structure. This barrier is either due to constrictions in the porosity of similar size to that of the adsorptive or a surface diffusion barrier. If constrictions are present in the porosity, the adsorption kinetic parameters will be markedly affected by the size of the adsorptive relative to the pore constrictions as observed for probe molecule studies of adsorption on carbon molecular sieves. Comparisons must take into account the surface coverage because the kinetics change with surface coverage. The decrease in adsorption rate constants with relative pressure for both *n*-nonane and α-pinene adsorption on MCM-41 at low surface coverage contrasts with the rate constants for nitrogen adsorption, which increase slightly, reaching a plateau at ∼25% pore filling. The pore volume data for *n*-nonane and α-pinene are very similar indicating the absence of constrictions in the porosity in the 400−700 pm size range. At low surface coverage, the rate constants for α-pinene are greater than for *n*-nonane at 313 K. Because α-pinene has a much larger minimum cross-sectional area than *n*-nonane (see Table 1) and has faster rate constants at low surface coverage, it is unlikely that constrictions influence the adsorption kinetics in this study.

Isotherm modeling studies have indicated that a simple one-dimensional homogeneous model gives a poor representation of the nitrogen adsorption isotherm for MCM-41 especially at low surface coverage. An improved representation of the nitrogen adsorption isotherm was obtained with a two-dimensional solid fluid potential that fluctuated greatly around the pore wall.[64] Adsorption and small-angle X-ray and neutron diffraction results have indicated[65] that at high resolution, the surface is smooth on the 400−700 pm scale with a fractal dimension of 2. At lower resolution, a fractal dimension of ∼3 was obtained, suggestive of rougher or uneven surfaces at greater than molecular dimensions, which are dissimilar. This was interpreted as being due to constrictions in the mesopore channels.[65]

Therefore, there is no strong evidence for kinetic limitations due to constrictions in the porosity although there are indications of heterogeneous surface effects. Therefore, the most likely explanation is that a surface diffusion barrier controls the adsorption kinetics at low surface coverage.

High Surface Coverage. The rate constants for adsorption of nitrogen, *n*-octane, and α-pinene on the precipitated silica (M001) and on MCM-41 show different trends with relative pressure. A minimum in the rate constant versus relative pressure graph is observed for adsorption of nitrogen, *n*-nonane, and α-pinene on MCM-41 at high surface coverage. This minimum is not observed for adsorption of these adsorptives on the precipitated silica M001. Therefore, the effect is related to the mesopore structure of MCM-41 and it occurs for adsorptives with markedly different shapes and sizes (see Table 1). The minimum occurs at ∼70% of the total pore volume obtained from the plateau for nitrogen adsorption, which has a slightly higher pore volume than either *n*-nonane or α-pinene. In the cases of *n*-nonane and α-pinene adsorption, the minima occurred at ∼60−65% of the corresponding total pore volumes for both adsorptives. It is apparent that the values for all three adsorptives are similar. The alignment of long thin molecules such as *n*-nonane ($401.4 \times 452.4 \times 1407.6$ pm) in the mesoporosity to produce pore blocking can be envisaged. However, if nitrogen ($299.1 \times 333.9 \times 536.1$ pm)[53] and bulky α-pinene (677×691 pm)[55] are considered in relation to the pore diameter (2.88 nm) determined from X-ray diffraction measurements, it is surprising that the same effect is observed. A comparison of the rate constants versus surface coverage calculated as a fraction (%) of total pore volume for nitrogen (77 K), *n*-nonane (313 K), and α-pinene (313 K) is shown in Figure 11. It is apparent that there are minima in the rate constant graphs for all three adsorptives in the region where mesopore filling is close to completion in MCM-41. This observation for adsorptives with a wide range of size and shape indicates a pore blocking effect due to cooperative effects, which is general in these ordered

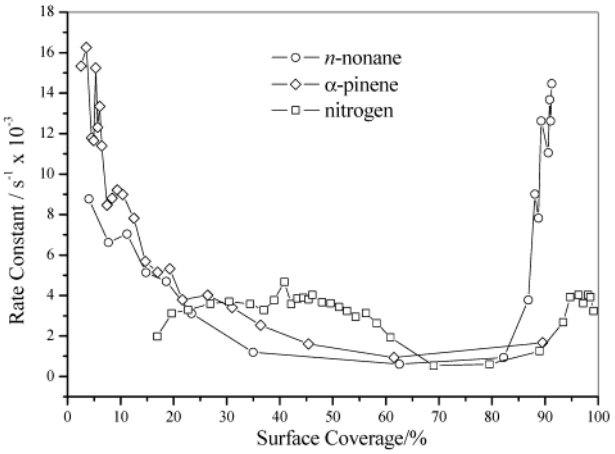

Figure 11. Variation of rate constant with surface coverage for adsorption of nitrogen (□, 77 K), *n*-nonane (○, 313 K), and α-pinene (◇, 313 K) on MCM-41.

mesoporous materials. A small increase in nitrogen pore volume was observed after adsorption of both *n*-nonane and α-pinene. No marked changes in the trends in nitrogen adsorption kinetic parameters were observed (see Figure 10), indicating that the pore blocking effect was unaffected by the small structural relaxation.

The adsorption kinetics for water vapor adsorption on active carbons, which have either type III or type V isotherms, also show a decrease in the rate constant with increasing surface coverage. This has been attributed to the formation of water molecule clusters around functional groups which causes the development of barriers to diffusion and hence, a decrease in the rate constants.[42,43]

5. Conclusions

Comparison of the pore volume data for nitrogen, carbon dioxide, *n*-nonane, and α-pinene for both M001 and MCM-41 show a weak trend: nitrogen > carbon dioxide > *n*-nonane ∼ α-pinene. The adsorption kinetic results obey the LDF model and are consistent with diffusion through a barrier being the rate-determining step regardless of the large variation in the size, shape and structure of the adsorptives. There are two possible barriers, either a surface barrier or diffusion through molecular size constrictions in the porosity. The observation of slower rate constants at low surface coverage for adsorption of *n*-nonane compared with the much larger α-pinene on MCM-41 indicates that constrictions in the porosity are not the rate-determining factor. It is proposed that a surface barrier to diffusion is present rather than constrictions in the pores.

Minima in the rate constants for adsorption on MCM-41 are observed for the adsorptives, which have markedly different size, shape, and structure, and for widely different adsorption temperatures. These minima are associated with the part of the isotherm where cooperative effects in filling the mesoporosity occur. This suggests a mesopore blocking mechanism, which is general for adsorption in this type of ordered mesoporous material.

Acknowledgment. We thank Dr. C. E. Webster, Texas A & M University, the late Dr. M. C. Zerner of the University of Florida, and Dr. Ted A. O'Brien of the University of Indiana for the calculations of the molecular dimensions of the adsorptives, and the EU for support for study leave for A.B.-M. at University of Newcastle upon Tyne under the Erasmus scheme.

Supporting Information Available: SEM data are available free of charge via the Internet at http://pubs.acs.org.

References and Notes

(1) Yanagisawa, T.; Shimizu, T.; Kuroda, K.; Kato, C. *Bull. Chem. Soc. Jpn.* **1990**, *63*, 988.
(2) Kresge, C. T.; Leonowicz, M. E.; Roth, W. J.; Vartuli, J. C.; Beck, J. S. *Nature* **1992,** *359*, 710.
(3) Beck, J. S. *US Patent 5057296*, **1991**.
(4) Beck, J. S.; Vartuli, J. C.; Roth, W. J.; Leonowicz, M. E.; Kresge, C. T.; Schmitt, K. D.; Chu, C. T. W.; Olson, D. H.; Sheppard, E. W.; McCullen, S. B.; Higgins, J. B.; Schlenker, J. L. *J. Am. Chem. Soc.* **1992**, *114*, 10835.
(5) Beck, J. S.; Vartulli, J. C. *Curr. Opin. Solid State Mater. Sci.* **1996**, *1*, 76.
(6) Kruk, M.; Jaroniec, M. *Chem. Mater.* **2001**, *13*, 3169.
(7) Cheng, C. F.; Zhou, W.; Park, D. H.; Klinowski, J.; Hargreaves, M.; Gladden, L. F. *J. Chem. Soc., Faraday Trans.* **1997**, *93*, 359.
(8) Ryoo, R.; Kim, J. M. *J. Chem. Soc., Chem. Commun.* **1995**, *7*, 711.
(9) Ciesla, U.; Schüth, F. *Micropor. Mesopor. Mater.* **1999**, *27*, 131.
(10) Raman, N. K.; Anderson, M. T.; Brinker, C. *J. Chem. Mater.* **1996**, *8*, 1682.
(11) Sayari, A.; Hamoudi, S. *Chem. Mater.* **2001**, *13*, 3151.
(12) Sayari, A. *Stud. Surf. Sci. Catal.* **1996**, *102*, 1.
(13) Sayari, A.; Liu, P. *Micropor. Mater.* **1997**, *12*, 149.
(14) Sayari, A. *Chem. Mater.* **1996**, *8*, 1840.
(15) Ying, J. Y.; Mehnert, C. P.; Wong, M. S. *Angew. Chem., Int. Ed.* **1999**, *38*, 56.
(16) Maschmeyer, T. *Curr. Opin. Solid State Mater. Sci.* **1998**, *3*, 71.
(17) Brunel, D. *Micropor. Mesopor. Mater.* **1999**, *27*, 329.
(18) Moller, K.; Bein, T. *Chem. Mater.* **1998**, *10*, 2950.
(19) Stein, A.; Melde, B. J.; Schroden, R. C. *Adv. Mater.* **2000**, *12*, 1403.
(20) Corma, A. *Chem. Rev.* **1997**, *97*, 2373.
(21) Branton, P. J.; Hall, P. G.; Sing, K. S. W. *J. Chem. Soc., Chem. Commun.* **1993**, *16*, 1257.
(22) Branton, P. J.; Hall, P. G.; Treguer, M.; Sing, K. S. W. *J. Chem. Soc., Faraday Trans.* **1995**, *91*, 2041.
(23) Franke, O.; Schulz-Ekloff, G.; Rathousky, J.; Stárek, J.; Zukal, A. *J. Chem. Soc., Chem. Commun.* **1993**, *9*, 724.
(24) Kruk, M.; Jaroniec, M.; Kim, J. M.; Ryoo, R. *Langmuir* **1999**, *15*, 5279.
(25) Liepold, A.; Roos, K.; Reschetilowski, W.; Esculcas, A. P.; Rocha, J.; Philippou, A.; Anderson, M. W. *J. Chem. Soc., Faraday Trans.* **1996**, *92*, 4623.
(26) Sonwane, C. G.; Bhatia, S. K.; Calos, N. *Ind. Eng. Chem. Res.* **1998**, *37*, 2271.
(27) Ribeiro-Carrott, M. M. L.; Candeias, A. J. E.; Carrott, P. J. M.; Ravikovitch, P. I.; Neimark, A. V.; Sequeira, A. D. *Micropor. Mesopor. Mater.* **2001**, *47*, 323.
(28) Sonwane, C. G.; Bhatia, S. K. *Langmuir* **1999**, *15*, 2809.
(29) Kruk, M.; Jaroniec, M.; Yang, Y.; Sayari, A. *J. Phys. Chem. B* **2000**, *104*, 1581.
(30) Edler, K. J.; Reynolds, P. A.; Branton, P. J.; Trouw F. R.; White, J. W. *J. Chem. Soc., Faraday Trans.* **1997**, *93*, 1667.
(31) Storck, S.; Bretinger, H.; Maier, W. H. *Appl. Catal. A* **1998**, *174*, 137.
(32) Ravikovitch, P. I.; Wei, D.; Chueh, W. T.; Haller, G. L.; Neimark, A. V. *J. Phys. Chem. B* **1997**, *101*, 3671.
(33) Braymer, T. A.; Coe, C. G.; Farris, T. S.; Gaffney, T. R.; Schork, J. M.; Armor, J. N. *Carbon* **1994**, *32*, 445.
(34) LaCava, A. I.; Dominguez, J.; Cardenas, J. *Ads. Sci. Technol.* **1988**, *158*, 323.
(35) LaCava, A. I.; Koss, V. A.; Wickens, D. *Gas Sep. Purif.* **1989**, *3*, 180.
(36) Dominguez, J. A.; Psaras, D.; LaCava, A. I. *AIChE Symp. Ser* **1988**, *84*, 73.
(37) Rutherford, S. W.; Do, D. D. *Langmuir* **2000**, *16*, 7245.
(38) O'Koye, I. P.; Benham, M.; Thomas, K. M. *Langmuir* **1997**, *13*, 4054.
(39) Reid, C. R.; O'koye, I. P.; Thomas, K. M. *Langmuir* **1998**, *14*, 2415.
(40) Reid, C. R.; Thomas, K. M. *Langmuir* **1999**, *15*, 3206.
(41) Reid, C. R.; Thomas, K. M. *J. Phys. Chem. B* **2001**, *105*, 10619.
(42) Harding, A. W.; Foley, N. J.; Norman, P. R.; Francis, D. C.; Thomas, K. M. *Langmuir* **1998**, *14*, 3858.
(43) Foley, N. J.; Forshaw, P. L.; Thomas, K. M.; Stanton, D.; Norman, P. R. *Langmuir* **1997**, *13*, 2083.
(44) Fletcher, A. J.; Thomas, K. M. *Langmuir* **1999**, *15*, 6908.

(45) Fletcher A. J.; Thomas, K. M. *Langmuir* **2000**, *16*, 6253.
(46) Fletcher A. J.; Benham, M. J.; Thomas K. M. *J. Phys. Chem. B* **2002**, *106*, 7474.
(47) Fletcher, A. J.; Cussen, E. J.; Prior, T. J.; Rosseinsky, M. J.; Kepert, C. J.; Thomas, K. M. *J. Am. Chem. Soc.* **2001**, *123*, 10001.
(48) Grün, M.; Unger, K. K.; Matsumoto, A.; Tsutsumi, K. *Micropor. Mesopor. Mater.* **1999**, *27*, 201.
(49) Benham, M. J.; Ross, D. K. *Z. Phys. Chem.* **1989**, *163*, 25.
(50) *Lange's Handbook of Chemistry*, 15th ed.; McGraw-Hill: New York, 1999.
(51) CRC *Handbook of Chemistry and Physics*, 74th ed.; CRC Press: Boca Ratan, FL, 1993.
(52) Fenelonov, V. B.; Romannikov, V. N.; Derevyankin, A. Yu. *Micropor. Mesopor. Mater.* **1999**, *28*, 57.
(53) Webster, C. E.; Drago, R. S.; Zerner, M. C. *J. Am. Chem. Soc.* **1998**, *120*, 5509.
(54) Webster, C. E.; Zerner, M. C. Personal communication.
(55) Webster, C. E.; O'Brien, T. A. Personal communication.
(56) Ainscough, A. N.; Dollimore, D. *Langmuir* **1987**, *3*, 708
(57) Yu, J.; Shi, J.-L.; Wang, L.-Z.; Ruan, M.-L.; Yan, D.-S. *Mater. Lett.* **2001**, *48* (2), 112.
(58) Freeman, J. J.; Tomlinson, J. B.; Sing, K. S. W.; Theocharis, C. R. *Carbon* **1993**, *31*, 865.
(59) Mueller, U.; Unger, K. K. In *Studies in Surface Science and Catalysis: Characterization of Porous Solids 1*; Unger, K. K., Rouquerol, J., Sing, K. S. W., Kral, H., Eds.; Elsevier: Amsterdam, 1987; Vol. 39, p 101.
(60) Yuzak, Y.; Zhao, X.; Thomas, K. M. Unpublished results.
(61) Rao, M. B.; Jenkins, R. B.; Steele, W. A. *Extended Abstracts, Biennial Conference on Carbon*; American Carbon Society: Lexington, KY, 1985; Vol. 17, p 114.
(62) Rao, M. B.; Jenkins, R. G.; Steele, W. A. *Langmuir* **1985**, *1*, 137.
(63) Chagger, H. K.; Ndaji, F. E.; Sykes, M. L.; Thomas, K. M. *Carbon* **1995**, *33*, 1405.
(64) Maddox, M. W.; Olivier, J. P.; Gubbins, K. E. *Langmuir* **1997**, *13*, 1737.
(65) Sonwane, C. G.; Bhatia, S. K.; Calos, N. J. *Langmuir* **1999**, *15*, 4603.